Research Article

Effects of Gamma Irradiation for Sterilization on Aqueous Dispersions of Length Sorted Carbon Nanotubes

Jeffrey A. Fagan[1] (✉), Nancy J. Lin[1], Rolf Zeisler[2], and Angela R. Hight Walker[3]

[1] Polymers Division, National Institute of Standards and Technology, Gaithersburg, MD 20899, USA

[2] Analytical Chemistry Division, National Institute of Standards and Technology, Gaithersburg, MD 20899, USA

[3] Optical Technology Division, National Institute of Standards and Technology, Gaithersburg, MD 20899, USA

© Tsinghua University Press and Springer-Verlag Berlin Heidelberg 2011

ABSTRACT

There is currently great interest in the potential use of carbon nanotubes as delivery vessels for nanotherapeutics and other medical applications. However, no data are available on the effects of sterilization methods on the properties of nanotube dispersions, the form in which most medical applications will be processed. Here we show the effects of gamma irradiation from a ^{60}Co source on the dispersion and optical properties of single-wall carbon nanotubes in aqueous dispersion. Samples of different length-refined populations were sealed in ampoules and exposed to a dose of approximately 28 kGy, a level sufficient to ensure sterility of the dispersions. In contrast to literature results for solid-phase nanotube samples, the effects of gamma irradiation on the dispersion and optical properties of the nanotube samples were found to be minimal. Based on these results, gamma irradiation appears sufficiently non-destructive to be industrially useful for the sterilization of nanotube dispersions.

KEYWORDS

1. Introduction

Single-wall carbon nanotubes (SWCNTs) display a unique range of material properties that are of interest for a variety of electronic [1], optical [2], and biomedical applications [3–8]. However, an unaddressed requirement for many of these projected uses, such as in targetable therapeutics [3–5] or contrast agents [7–9] is the necessity to deliver the materials in a sterile form. A typical method for sterilizing materials is irradiation. To date there have been relatively few literature reports of the effect of irradiation in general on the properties of nanotube powders [10], films [11–16] or devices [15, 16],

and no reports of the effects on dispersed nanotubes. This information is most lacking in the case of the effects of a common sterilization procedure, gamma irradiation [17, 18], as opposed to electron[19, 20] or ion irradiation[11, 14]. The effects of the sterilization will be of particular importance for separated SWCNT populations, as the length [21, 22], chirality [23], and potentially specific enantiomers [24] will likely be selected to maximize efficacy in the regulated applications for which sterilization will be required. Separated populations of nanotubes have additional processing concerns that currently require the nanotubes to be kept in the liquid phase to avoid dramatic

Address correspondence to Jeffrey.fagan@nist.gov

alteration to the dispersed morphology or substantial mass loss on redispersion.

Gamma irradiation from a ^{60}Co source is a common industrial technique for the sterilization of many materials, from foodstuffs such as ground beef to biomedical devices. The low cost, high penetration ability, and the possible sensitivity of nanotube solutions to other sterilization techniques [10] such as heat, filtration, UV irradiation, gas plasma [25], and pressure treatments, make gamma irradiation the most likely route for the sterilization of nanotubes. However, gamma sterilization was previously found to alter the measured Raman scattering of a nanotube powder [10], and has also shown mixed effects in previous studies on other, primarily lyophilized, nanoparticles [26, 27]. Sterilization is achieved in gamma irradiation through the destruction of the genetic material in the affected cells, and may affect the properties of a nanotube sample through several mechanisms, including direct damage, indirect damage through reaction with induced free radicals [17, 28], disruption of the dispersion for liquid samples, or alteration of the adsorbed species on the dispersed SWCNTs. As the size, shape, surface coating, and aggregation state of a nanoparticle often directly influence its displayed or desired properties and its interaction with cells [4, 25, 26, 29, 30], any changes to these properties associated with sterilization will be of critical importance.

To measure potential changes in the properties of a nanotube dispersion due to irradiation, it is possible to use the nanotube optical properties, which are highly sensitive to the aggregation state, structural defect density, and the local chemical environment around the nanotube. To measure these properties there has been substantial development in using UV–visible–near infrared (UV–vis–NIR) absorbance, near infrared (NIR) fluorescence [31], and resonance Raman spectroscopy for nanotube populations. In this contribution we report the effects of gamma sterilization, as measured by these optical metrics, on a set of length-resolved populations of nanotubes in aqueous dispersion.

2. Results and discussion

The irradiated populations used in this study were processed by centrifugation and forced filtration to disperse and purify the nanotubes, perform length separation, and adjust the final solution conditions. After processing, the nanotube dispersions were dialyzed to 1.0% sodium deoxycholate (DOC) surfactant concentration and sealed into pre-cleaned glass ampoules. It should be noted that the processing for these purified and separated samples removes the non-nanotube components, including the nanotube catalyst. To confirm the removal of the catalyst, induced neutron activation analysis (INAA) was performed on 0.5 mL aliquots of the irradiated samples. The amounts of the primary catalyst components, Co and Mo [32] were below the limit of detection, < 5 mg/kg and < 40 mg/kg respectively on a dry mass basis, in both the Medium and Long fractions, and measured at 12 mg/kg ± 2 mg/kg and 47 mg/kg ± 11 mg/kg on a dry mass basis respectively in the Short fraction. For the least pure Short sample, comparing the amount of residual catalyst elements, ≈ 60 mg/kg, to the dry nanotube mass, ≈ 13,000 mg/kg, the purity of the nanotube component of the sample is calculated to be approximately 99.5%.

A picture of the irradiated length-separated nanotube dispersions is shown in Fig. 1. The samples were irradiated to an average dose of 28 kGy. A side effect of the irradiation, observed in Fig. 1, is that the previously clear glass ampoules became amber

Figure 1 Photograph of (left to right) the Long, Medium, and Short length-sorted nanotube dispersions after ampouling and gamma irradiation. The blank reference solution containing only 1% sodium deoxycholate is displayed to the right. The dispersions display a uniform appearance with no visible settling or aggregate formation. The irradiation process itself induces a yellowing of the initially clear glass ampoules

colored. Visual inspection of the irradiated liquids indicated no apparent change to the bulk appearance of either the actual samples that comprise RM 8281 (currently 11 months post irradiation), or for a draft fraction irradiated for process development (1 yr before measurement).

The irradiated nanotubes were confirmed to be sterile, via inoculation into growth media, for both aerobic and facultative anaerobic conditions in both liquid and agar plate cultures. Pictures of these tests recorded 7 days after inoculation onto agar plates and cultured in both aerobic and facultative anaerobic conditions are shown in Fig. 2. Similar results were found at earlier times and for liquid cultures (see Figs. S-1 and S-2 in the Electronic Supplementary Material (ESM)). None of the irradiated samples demonstrated any visual presence of growth at any time, for any of the conditions tested. Positive controls with *E. coli* or *S. mutans* had growth within 24 h, even in the presence of the greatest nanotube concentrations. The non-sterilized parent population also had growth, indicated by colony
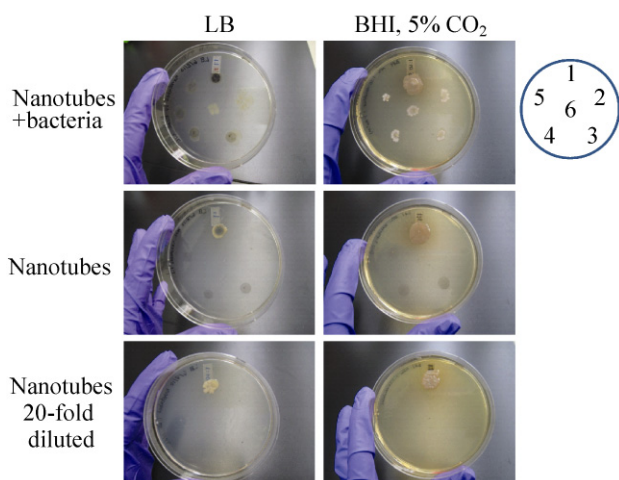

Figure 2 Representative images of agar plate cultures using LB (left) and BHI (right) after 7 days of culture. Image rows show samples that were spiked with bacteria, full strength samples, and 20-fold diluted samples. The key on the right identifies the positions of the nanotube samples as follows: (1) non-irradiated nanotube parent population, (2) irradiated 1% sodium deoxycholate reference, (3) irradiated Short nanotubes, (4) irradiated Medium nanotubes, (5) irradiated Long nanotubes, and (6) negative control (buffer). The non-irradiated parent sample shows growth despite high nanotube (≈ 1 mg/mL) and surfactant (2%) concentrations. The irradiated samples did not display growth, except when spiked with bacteria for the positive control

formation on the agar cultures, and turbidity and growth in the liquid cultures within 48 h for both the aerobic and facultative anaerobic conditions. Although no bulk change in appearance has been observed in the parent solution over a one year timeframe, this result indicates the necessity for sterilization of nanotube dispersions, even when the dispersion properties (2% DOC, ≈ 1 mg/mL nanotubes) would be expected to be hostile to bacterial contamination. Although it is possible that sample processing prior to irradiation eliminated the contamination present in the parent dispersion, the sterility testing conclusively demonstrates that any contaminants that might have been present in the samples at the time of irradiation are no longer viable. It is likely that the amount of irradiation used in the processing of these samples was greater than the necessary dosage to ensure sterility. It has been reported that sterilization of doxorubicin bound to butylcyanoacrylate nanoparticles could be achieved to European Pharmacopeia regulatory standards with a 15 kGy or lower dose [18], substantially below the 28 kGy dose applied in this study.

An alternative strategy for the irradiation of the dispersions involves the pre-sterilization of the raw nanotube powder [10] by a variety of techniques including irradiation, ethylene treatment, and UV exposure, or [12] gamma irradiation, followed by processing in a sterile environment. This approach was not chosen for several reasons: the difficulty in maintaining sterile conditions given the amount of processing performed in the purification and length separation of the material; the potential for variable exposure of the granular nanotube powder to the different techniques [10]; the lack of data in the literature on the effects of these procedures; the possibility of variation in effects due to soot composition; and the definitiveness of post-ampouling sterilization. Dispersion-based purification and liquid phase processing followed by filtration and sterilization of a solid sample prior to redispersion was dismissed for similar reasons, although the primary reason was our experience that the redispersion of purified SWCNTs is technically challenging and is accompanied by a significant, > 50%, mass loss.

Comparison of the optical absorbance of the dispersions before and after ampouling and gamma

irradiation is shown in Fig. 3. For SWCNTs, the location and strength of the optical transitions in the absorbance spectra is a sensitive function of the distribution of chiralities in the sample, the local chemical environment at the nanotube interface, solution purity, and the length of the nanotubes. The absorbance spectra of the nanotubes (Fig. 3(a)) were relatively unchanged by the irradiation process. This lack of change is evident in the nearly overlapping spectra recorded before and post irradiation; the most sensitive absorbance features are the first interband transitions of the nanotubes located in the NIR. It is immediately apparent from the optical spectra that the dispersion of the nanotubes was not greatly influenced by the irradiation. Significant flocculation in the irradiated sample would be measurable through an increase in the apparent absorbance at short wave-lengths (from the increased light scattering with larger particle size), as well as a general decrease in the absorbance at longer wavelengths. These phenomena are not apparent in the data. Larger versions of Figs. 3 and 4 are presented in Fig. S-6 (in the ESM), to emphasize the lack of any significant differences before and post irradiation.

Two significant changes were observed as effects of the irradiation, an increase in the UV absorbance of the surfactant solution, and a reduction in the strength of the first interband optical transitions of the semicon-ducting nanotubes (most evident for the (6,5) nanotube transition at 982 nm). The increased UV absorbance of the surfactant is likely evidence of a chemical change induced by the irradiation; the reduction in the strength of the optical transition could have several causes. The E_{11} transition of the semiconducting nanotubes is the most sensitive transition to the local dispersion state and chemical environment of the nanotubes. One method to quantify the optical strength per apparent dispersed nanotube mass is to measure the ratio of the peak absorbance of a feature compared to the baseline absorbance at a wavelength with little peak feature contribution. This is illustrated in Fig. 3(b) for the (6,5) nanotube absorbance; the decrease is $\approx 6\%$ for the Long sample, and less for the Medium and Short samples. Data are shown for the unampouled samples to demonstrate that the decrease in optical strength is not due to the ampouling process.
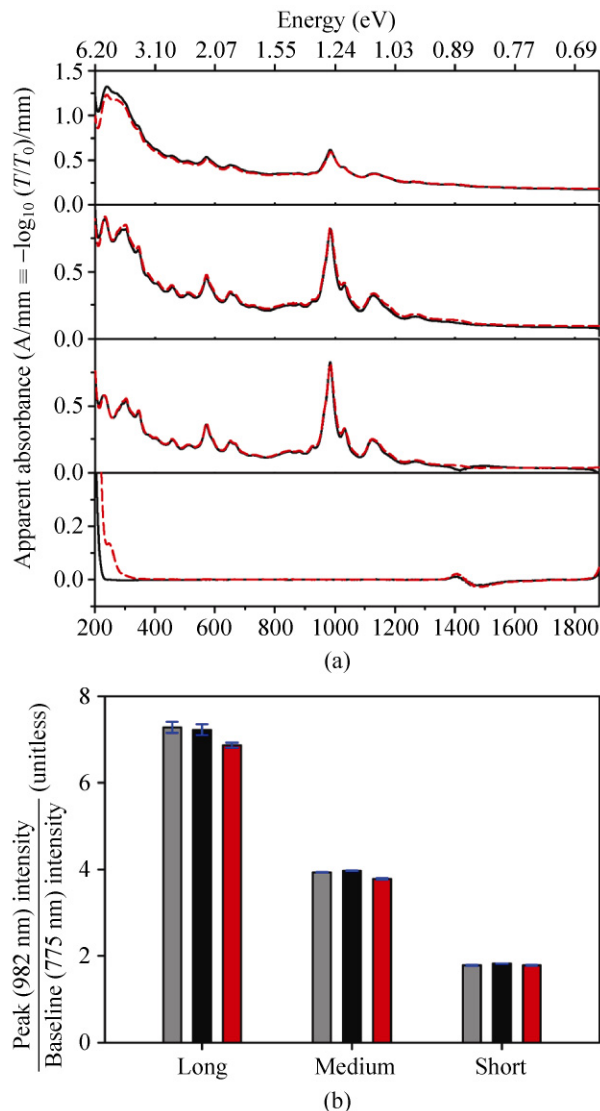

Figure 3 (a) UV–vis–NIR absorbance spectra for the three length-sorted dispersions, from top the Short, Medium, and Long fractions, and for reference the sodium deoxycholate solution before (solid, black curves) and after (dashed, red curves) ampouling and gamma irradiation. The nanotube spectra were corrected using the appropriate deoxycholate spectra; the deoxycholate spectra were corrected by subtracting the spectra of deionized (18 MΩ) water. The spectra of the nanotube dispersions were nearly equivalent after the processing, although the strength of the (6,5) nanotube E_{11} optical transition (982 nm) was decreased slightly in the Medium and Long fractions. The small effect of irradiation on the absorbance spectra indicates that the nanotube dispersion was not significantly altered by the processing. (b) Comparison of the peak absorbance of the (6,5) nanotube to the baseline absorbance at 775 nm, a metric for comparing optical strength per dispersed mass. Shown are measurements for preampouled (gray bars), ampouled (black bars), and ampouled and irradiated (red bars) samples. The irradiation decreases the ratio by less than $\approx 6\%$, with the largest decrease occurring for the Long fraction
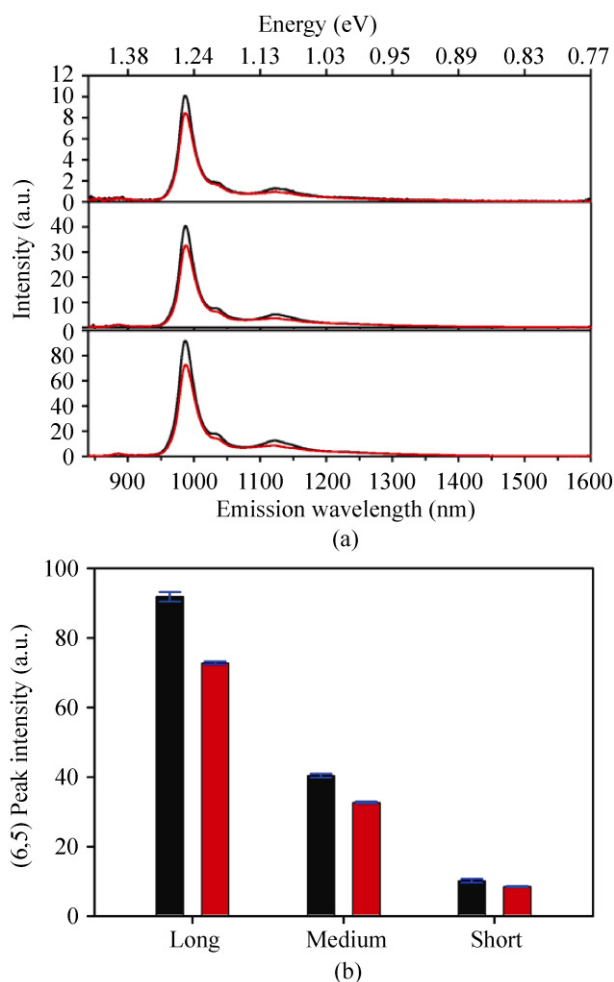
Figure 4 (a) Comparison of the NIR fluorescence measured for the three nanotube populations, from top Short, Medium, and Long, comprising NIST RM 8281 prior to (solid, black curves) and post (dashed, red curves) irradiation. The samples were diluted with surfactant–D$_2$O solution to a common absorbance of 0.04 cm^{-1} at 775 nm; the excitation wavelength was 568.5 nm. No peak shifts were observed with irradiation. (b) Peak emission intensity from the (6,5) nanotube in the non-irradiated (black bars) and irradiated (red bars) samples. The fluorescence of the (6,5) nanotube in each of the three fractions was reduced by as much as 21% by the gamma irradiation procedure

The most likely explanations for the reduced optical transition strength are the formation of small aggregates, reduced protection or an altered chemical environment at the nanotube interface with the environment due to the changes in the surfactant solution, and/or chemical functionalization of the nanotubes driven by the irradiation. To probe these possible changes to the nanotubes or the dispersion quality, three additional experiments were performed:

exchange of the irradiated nanotubes into fresh DOC solution; measurement of the NIR fluorescence of the nanotube dispersions; Raman scattering measurement of the G/D and radial breathing mode (RBM) ratios of the nanotubes.

To determine whether the decrease in the peak UV–vis–NIR absorbance was a function of an altered chemical environment due to changes in the dispersant, an ultrafiltration cell was used to exchange the bulk surfactant solution with non-irradiated stock solution. This experiment found no positive improvement of the peak to baseline absorbance. It should be noted that DOC was chosen initially as the surfactant because it had previously been found to be among the best dispersants for nanotubes [33], as measured by both the degree of individualization of the nanotubes [33, 34], and its ability to prevent aggregation of the individualized SWCNTs even at mass loadings above 1 mg/mL in solution. Moreover DOC and the related tri-hydroxy surfactant sodium cholate, are also the most commonly used surfactants for nanotube separations and processing [23]. However, as with most small molecule surfactants for nanotubes, a large fraction of the total surfactant concentration exists as a combination of small micelles and free molecules at a deoxycholate concentration of 1%, rather than on the nanotube surface. This likely provided a reservoir of undamaged surfactant, such that any damage to the adsorbed layer could be immediately repaired through exchange with the excess in solution. The availability of the excess surfactant in the bulk is a likely reason why no effect was seen on the nanotube absorbance with the exchange of the bulk solution.

Substitution of a different dispersing agent for the DOC, however, might result in differing amounts of damage to the nanotubes depending on the bulk concentration of the molecule and its susceptibility to reaction with radical species. This may particularly apply to polymeric dispersants such as DNA that do not need to be present in a significant excess in solution to stabilize the dispersion. It is possible that damage to the dispersant from the irradiation would more significantly affect the end properties of the nanotubes in this case. However, there are several strategies for preventing this damage, including the use of radical scavengers, or the post processing exchange of the DOC

to a different (pre-sterilized) dispersant that is more biocompatible, such as phospholipid-PEG [35].

Lastly, of importance to note in Fig. 3 is the significant intrinsic absorbance by the nanotubes in the UV region, 200 to 320 nm, despite nanotube concentrations of the order of 0.1 mg/mL. The large extinction coefficient of the nanotubes in this region reduces the potential for other possible sterilization techniques such as UV irradiation of SWCNT dispersions by severely limiting the penetration depth of the light. The utility of UV irradiation is further limited by the susceptibility of many biomolecules (such as DNA or protein-based targeting molecules) to UV-induced damage and the possibility of nanotube-induced photochemistry or photodegradation. The high penetration of gamma radiation from a ^{60}Co source, in contrast, enables bulk processing of liquid phase materials.

In addition to absorbance, other optical properties of SWCNTs can yield substantial information about their degree of defects and chemical environment. NIR fluorescence is a sensitive technique for probing the local environment and degree of structural non-uniformity of individualized SWCNTs. The presence of defects, non-uniform surface coatings [36–38], aggregation [38], and oxidizing chemical environments [39] are all known to diminish or extinguish nanotube fluorescence. A comparison of the fluorescence measured from the three nanotube populations prior to and post gamma irradiation is shown in Fig. 4, and a broad range excitation–emission contour plot is shown in Fig. S-3 in the ESM.

Disappointingly, the gamma irradiation process measurably decreased the NIR fluorescence of the nanotube samples. A decrease of ≈ 21% was measured at 988 nm (peak emission) with excitation at 568.5 nm for the Long fraction, with lower decreases of ≈ 19% and ≈ 16% measured for the Medium and Short samples respectively. However, since DOC-dispersed nanotubes are typically 2 to 3 times brighter than nanotubes dispersed by other dispersants [34], this decrease is not likely to be overtly harmful for fluorescence applications of the irradiated samples. Because each of the samples was diluted by a factor of approximately 30:1 (Long) to 100:1 (Short) with the D$_2$O surfactant solution it is unlikely that any damage to the surfactant coating by the irradiation would cause the decrease

in the fluorescence intensity. As the absorbance data also indicate that the quality of the dispersion is not substantially altered by the irradiation, the most likely explanation is that some quantity of optically active defects are generated on the nanotubes by the irradiation.

Gamma irradiation can cause damage either directly through the destruction of covalent bonds, or indirectly through the generation of free radicals in solution that react with the nanotubes to cause chemical functionalization [17]. C$_{60}$ molecules are known to be susceptible to functionalization in this manner [40]. In general, the effect of gamma irradiation on aqueous samples is to produce hydroxyl radicals (·OH) at a rate (G) of 0.28 µmol/J [28], although other species are also produced, and the type of radical can be affected by the presence of other molecules. Because the amount of radicals produced is generally relatively insensitive to the dispersed species, aqueous samples often show an inverse relationship between the percentage of the solute degraded and the solute concentration [41]. Although the nanotube concentration decreased with increasing length in the three samples, which is consistent with this observation, the surfactant concentration was equivalent in all samples at roughly 100x greater than the nanotube concentration. Thus, the differences in bulk nanotube concentration are unlikely to be the source of the different degrees of degradation observed in the three nanotube samples [28]. Instead, the observation likely indicates that the optical properties of the longer nanotubes were more sensitive to the incorporation of defects than the shorter nanotubes on a mass basis. This is expected because the exciton diffusion length in DOC has been measured as at least 240 nm [42]. Raman scattering is often used to evaluate the defect density of nanotube samples, of which added functional groups are a known contributor, although it is likely that not all fluorescence quenching defects are Raman active.

Raman scattering is the third commonly used optical technique to characterize SWCNTs [43]. In particular, three Raman scattering features are used to study nanotube structure: the RBM mode, which reflects the distribution of chiralities in resonance with the excitation wavelength; the D band, which is generated by scattering at a defect site; the G and G' bands, which

are fundamental modes seen in graphite. Often, the G/D and G′/D ratios are used to estimate the defect density in a sample. From previous measurements on length-sorted nanotubes, it is known that these ratios depend on the length L of the dispersed nanotube with a 1/L dependence due to ends of the nanotubes acting as defects [36]. Also notable is that the ratios vary with the excitation wavelength due to resonance effects. In Fig. 5(a), the Raman scattering for the region covering the D and G bands is shown for the three pairs of irradiated/unirradiated RM 8281 length fractions measured with 632.8 nm excitation. Similar D to G region scattering measured at 514.5 nm excitation is shown in Fig. S-4 (in the ESM). In Fig. 5(b), the G/D ratios from the data measured at both 514.5 nm and 632.8 nm are shown for the three pairs of fractions. Figure 5(c) displays the RBM region measured with 632.8 nm excitation for the three samples.

Unlike previously reported work [10], in which a raw nanotube powder was irradiated to an apparent dose of 10 Gy (1000 rad) over 3 min, relatively little change in the G/D ratio was observed for the dispersed samples studied here. For these samples the decrease was ≈ 5.5% for the Long sample, and ≈ 4.5% and ≈ 1.3% for the Medium and Short samples respectively. These changes are also much less than that observed for filtered bucky papers of SWCNTs in air [11], which showed an approximate 80% increase in the D band intensity (≈ 45% decrease in G/D ratio), although nearly twice the exposure (53 kGy) used in this latter study. This effect was reported to be reduced for bucky paper samples irradiated in a vacuum. Generation of covalent attachments to, or structural defects in, the nanotube lattice would explain both the decrease in the G/D scattering ratio and in the NIR fluorescence. However, it is unclear what percentages of these changes are due to the creation of additional Raman active defects on the nanotubes such as these, or contributions from other possible, but less likely, factors such as the decreasing of the length of the nanotubes in solution, the dependence on length of the effective scattering cross sections, and/or a decrease in resonance coupling to the optical transitions (because of the reduction in excitonic absorbance). The changes are conclusively not due, however, to a shifting of
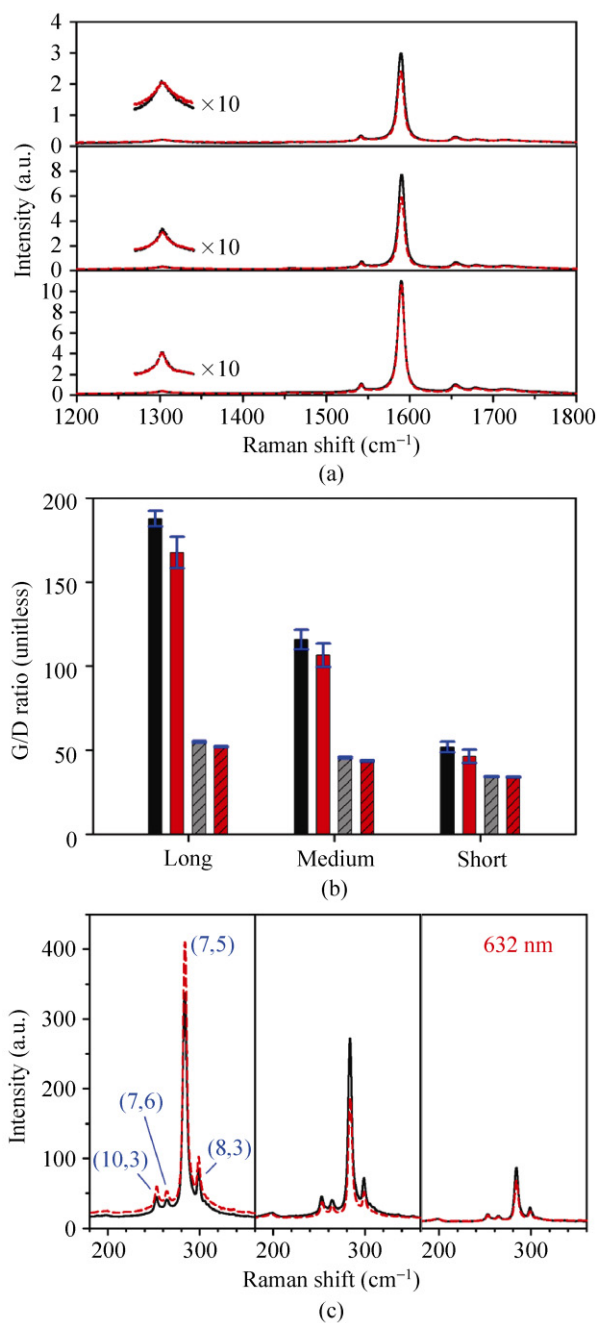

Figure 5 (a) Raman spectra for the wavenumber shift range including the D band (≈ 1330 cm^{-1}) and the G band (G$^+$ ≈ 1590 cm^{-1}, G$^-$ ≈ 1570 cm^{-1}) scattering from the irradiated (red, dashed line) and unirradiated (black, solid line) fractions (from top: Short, Medium, Long) measured at 632.8 nm excitation. (b) G/D ratios for the three pairs of length fractions (solid: 514.5 nm, crosshatch: 632.8 nm) before and post irradiation; error bars denote range of fit values. The G/D ratio of the irradiated fraction was consistently reduced by the processing. (c) Comparison of RBM modes for before and post irradiation pairs measured with 632.8 nm excitation. Little change was observed in the RBM distribution. Note that it is the intensity of the features relative to each other, and not the absolute intensity that is compared

resonance energies as no shifts in peak locations were observed in absorbance or fluorescence measurements.

The distribution of the RBM modes in the dispersed samples is also relatively unaffected by the irradiation process (Fig. 5(c)). This is again different from the results in the literature [10, 12], both of which used solid phase samples. However, the comparison for which the effect of irradiation was shown in one case [12] could represent an exposure of 170 kGy, much higher than that used in the current study. Diameter-selective damage has also been reported in solid phase samples from irradiation by soft X-rays and electrons [44]. The difference between the effect on dispersed samples in this study, and the solid samples [10, 12] could be due to several factors, the most likely of which is the fundamental difference in radiation chemistry for solid samples, which is dominated by direct ionization of the material, whereas for aqueous liquids the reaction with radical species such as ·OH is the dominant mechanism for damage to a solute [45]. The elimination of non-nanotube constituents in the length-sorted fractions, and superior heat transfer in an aqueous dispersion as compared to a low density solid may also contribute to the observed differences. Further work is also necessary to determine if the diameter distribution of the population affects the response to irradiation. Raman spectra covering the whole measured wave-number shift range are shown in Fig. S-3 in the ESM.

3. Conclusions

The irradiation of a set of nanotube samples in aqueous dispersion is demonstrated to ensure sterility of the ampouled liquid, while substantially maintaining the dispersion and optical properties of the dispersed nanotubes. The most significant changes to the optical properties, decreases in the peak absorbance, fluorescence, and Raman G/D ratios of ≈ 6%, ≈ 21%, and ≈ 5.5% respectively, are likely acceptable for most applications. These changes were demonstrated to occur due to direct damage or chemical functionalization of the nanotubes, and not due to an environmental change. The greatly reduced damage measured for the samples in this study, as compared to the previous reports on solid phase samples, indicates that liquid phase sterilization is a valuable processing strategy. Further-

more, it is likely that the amount of irradiation used in this study was significantly more than required to ensure sterility of the dispersions. Less irradiation or use of additives that scavenge free radicals during irradiation should further reduce the effects to the optical properties.

4. Methods

Aqueous dispersions of length-sorted carbon nanotubes were generated for the production of the National Institute of Standards and Technology (NIST) reference material (RM) 8281 "Length Separated Carbon Nano-tubes in Liquid Dispersion". A comprehensive report of the properties and preparation of this material will be upon available free of charge upon release of the material at www.nist.gov. Briefly, a SWCNT soot from the cobalt–molybdenum-catalyst (CoMoCat) production method (Southwest Nanotechnologies, SG65-000-0024) [46] was dispersed into 2% (mass/volume) DOC solution through tip sonication (1 h, ≈ 1 W/mL, 1 mg/mL nanotube concentration) in a 50 mL centrifuge tube immersed in an ice bath. Subsequently large bundles of nanotubes and non-nanotube impurities were removed through a centrifugation step (JA-20 rotor, 2 h, 1885 Rad/s) after which the supernatant was collected. This liquid was the parent dispersion for length separation.

Length separation of the nanotube populations was accomplished through exploiting the difference in the sedimentation rate with length for rods in an ultracentrifuge [47, 48] (SW-32, 21 h, 2650 Rad/s). Thirteen fractions were collected post centrifugation. Several fractions of similar lengths were subsequently combined and purified to remove the iodixanol density medium and to form three fractions, a Long, Medium, and Short. The ultrafiltration cell used to reduce iodixanol content was simultaneously used to reduce the surfactant concentration to 1%. The final iodixanol concentration, extrapolated from the iodine concentration measured by elemental analysis, was ≈ 5 μg/mL or less in all the nanotube-containing samples. After the fractions were finalized, the three fractions plus a 1% sodium deoxycholate solution from the same lot were ampouled into precleaned borosilicate glass ampoules (≈ 2.5 mL) and sealed under argon gas.

Ampoules were then selected for retention as is, or for irradiation on the basis of a randomized sampling plan.

Gamma irradiation (primary decay of ^{60}Co produces irradiation $\gamma = 1.17$ MeV and 1.33 MeV) was performed by Neutron Products at their facility in Dickerson, Maryland. A range of the irradiation dose for the ampouled samples was reported as 27.7 to 35.1 kGy; the dose rate was 2.09 kGy/h. One Gray (Gy) is defined as 1 J/kg absorbed dose. A screening test on a similarly prepared lot of separated nanotubes processed by Neutron Products a year earlier to a level of 26.0 to 28.3 kGy indicated this was an acceptable dose that would not dramatically alter the properties of the dispersed nanotubes. The reported measurement uncertainty on the absorbed dose as measured by FWT60-00 dosimeters was reported as $\pm 4.0\%$ at a 95% confidence level. Prior to, and post irradiation, ampoules were stored at laboratory room temperature; monitoring by irreversible temperature sensor labels recorded no excursions from the range of 0 to 37 °C.

Quantitative elemental analysis was carried out by INAA using previously implemented procedures for the characterization of the bulk starting material, which is to be issued as SRM 2483 [32], from which the samples in this contribution were produced. Briefly, 0.5 mL aliquots from fresh sample ampoules were pipetted into bags made from 6.3 μm thick polypropylene film and dried. The samples were irradiated together with known standard samples and blanks and were measured under the same conditions according to the INAA comparator method [49]. Several measurements were made for each sample for broadest elemental coverage. Concentrations are reported based on the total dry mass, except where otherwise noted, which was taken to be 1.0% of the measured mass of the aliquot added to the polypropylene bag.

Sterility of irradiated nanotube populations was evaluated via liquid and agar plate cultures under two growth conditions [50]: Luria–Bertani (LB) medium in aerobic conditions (with shaking for the liquid cultures), and brain heart infusion (BHI) medium in reduced oxygen conditions (5% CO_2 incubator, static cultures). All cultures were maintained at 37 °C. These conditions were selected to test for presence of a variety of microbial contaminants, including aerobes and facultative anaerobes. Samples tested included

the non-irradiated nanotube parent population, the irradiated ampoules of Long, Medium, and Short nanotubes, and the irradiated 1% sodium deoxycholate reference. Two concentrations of nanotubes were used to inoculate the growth media, as irradiated and 20-fold diluted in phosphate buffered saline (PBS), to discount the possibility that a potential contaminant species could be inhibited by the nanotube concentration in the full-strength samples. For all liquid cultures, 50 μL of sample (either undiluted or 20-fold diluted) was added to 3 mL of liquid medium in a 15 mL centrifuge tube. For all agar cultures, 10 μL of sample were spotted on the agar plate. Sterile PBS was used as a negative control. Positive controls for the growth conditions were demonstrated through addition of live bacteria to some samples for each condition. For the liquid and agar LB positive controls, *Escherichia coli (E. coli)* K-12 strain SF2086 was added to the samples by inoculation with a 10^{-6} dilution of an overnight culture grown in LB. For the BHI liquid and agar positive controls, the facultative anaerobe *Streptococcus mutans (S. mutans)* Clarke UA159 from the American Type Culture Collection (ATCC) was added at a 10^{-3} dilution of an overnight culture grown in BHI. All samples and controls were tested in triplicate for each culture condition. Cultures were visually inspected for growth for 7 days. Positive growth was defined as colony formation on the agar cultures, and by the observation of turbidity in the liquid cultures. Turbidity measurements via optical density, a common way to determine growth in liquid cultures, were not utilized due to the presence of the nanotubes. Digital images of the cultures were taken on days 3 and 7.

UV–Vis–NIR experiments were made in transmission geometry on a PerkinElmer Lambda 950 UV–Vis–NIR spectrophotometer over a wavelength range of 1880 to 185 nm. The incident light was circularly polarized prior to the sample compartment, and the spectra corrected for both dark current and background. The optical absorption spectra were recorded at 1 nm increments with an instrument integration time of at least 0.16 s per increment using a 1 mm pathlength quartz cuvette. The reference beam was left unobstructed, and the subtraction of the appropriate reference sample was performed during data reduction.

NIR fluorescence spectra were measured using a

HORIBA Jobin Yvon NanoLog-3 spectrofluorometer with a liquid nitrogen cooled InGaAs array detector and a 450 W xenon lamp. Excitation was selected using a dual grating monochromator with 1200 × 500 gratings, and a slit selected bandpass of 5 nm (single wavelength measurements) or 8 nm (excitation versus emission contour plot). Emission was measured in the right angle geometry with a 10 mm square quartz cuvette through a long-pass filter and dispersed with a 100 × 800 grating onto the array detector. Bandpass for the emission side was set to 8 nm. Most measurements were collected using excitation at 568.5 nm, which was measured to produce the largest (6,5) emission, for 90 s. For large wavelength range acquisitions, excitation was stepped in 5 nm increments with an integration time of 45 s. Collected spectra were corrected for the wavelength-dependent irradiance of the excitation beam, and the wavelength dependence of the long pass filter and detector train as calibrated to a NIST traceable lamp. To account for differences in concentration of the fractions, all fractions were diluted to a common absorbance of 0.04/cm at 775 nm using a solution of 1% sodium deoxycholate in D_2O. At this dilution, peak locations can be measured with minimal in-filter effects, however the comparison of the absolute intensities of emission at different wavelengths may still be affected.

The spontaneous Raman backscattered light was collected in a collinear 180° backscattering configuration with a triple grating spectrometer (Dilor XY800) and a liquid nitrogen cooled CCD detector. An Ar^+ laser (Coherent Innova Sabre with multiline visible head) provided the 514.5 nm excitation, and a HeNe laser was used to provide the excitation at 632.8 nm; in each case approximately 15 mW of power was focused to a spot size of approximately 100 μm within the liquid sample volume. Cyclohexane was used as a reference standard to ensure wavenumber accuracy. Raman frequency shifts in the range from approximately 100 to 3600 cm^{-1} were measured at 514.5 nm excitation, which covers the region of spectral shift in which RBM, D band, G band, G′ (2D), and water Raman features occur; specific spectral windows to cover the RBM, D, G, and G′ modes were measured at 632.8 nm. The integration time for the fractions was 45 to 180 s averaged over 3 scans for the D and G band region,

measuring longer for the shorter fractions. The G/D ratio was calculated using the peak values of the G and D features after subtraction of a linear and sloped background respectively. The backgrounds were taken as the non-resonant signal averaged from 1270 to 1273 cm^{-1} for the G band, and as sloped line between the measured signal averaged over the region 1270 to 1285 cm^{-1} and the average over the region from 1380 to 1400 cm^{-1}. RBMs were assigned using [51].

Unless otherwise noted, the standard uncertainty is denoted in this contribution through error bars representing one standard deviation.

Acknowledgements

References

[1] Wu, Z. C.; Chen, Z. H.; Du, X.; Logan, J. M.; Sippel, J.; Nikolou, M.; Kamaras, K.; Reynolds, J. R.; Tanner, D. B.; Hebard, A. F.; Rinzler, A. G. Transparent, conductive carbon nanotube films. *Science* **2004**, *305*, 1273–1276.

[2] Kymakis, E.; Amaratunga, G. A. J. Single-wall carbon nanotube/conjugated polymer photovoltaic devices. *Appl. Phys. Lett.* **2002**, *80*, 112–114.

[3] Kam, N. W. S.; O'Connell, M.; Wisdom, J. A.; Dai, H. J. Carbon nanotubes as multifunctional biological transporters and near-infrared agents for selective cancer cell destruction. *Proc. Natl. Acad. Sci. USA* **2005**, *102*, 11600–11605.

[4] Lacerda, L.; Bianco, A.; Prato, M.; Kostarelos, K. Carbon nanotubes as nanomedicines: From toxicology to pharmacology. *Adv. Drug Deliv. Rev.* **2006**, *58*, 1460–1470.

[5] Xiao, Y.; Gao, X.; Taratula, O.; Treado, S.; Urbas, A.; Holbrook, R. D.; Cavicchi, R. E.; Avedisian, C. T.; Mitra, S.; Savla, R.; Wagner, P. D.; Srivastava, S.; He, H. Anti-HER2 IgY antibody-functionalized single-walled carbon nanotubes for detection and selective destruction of breast cancer cells. *BMC Cancer* **2009**, *9*, 351.

[6] Besteman, K.; Lee, J. O.; Wiertz, F. G. M.; Heering, H. A.; Dekker, C. Enzyme-coated carbon nanotubes as single-molecule biosensors. *Nano Lett.* **2003**, *3*, 727–730.

[7] Barone, P. W.; Baik, S.; Heller, D. A.; Strano, M. S. Near-infrared optical sensors based on single-walled carbon nanotubes. *Nat. Mater.* **2005**, *4*, 86–92.

[8] Ananta, J. S.; Matson, M. L.; Tang, A. M.; Mandal, T.; Lin, S.; Wong, K.; Wong, S. T.; Wilson, L. J. Single-walled carbon nanotube materials as T2-weighted MRI contrast agents. *J. Phys. Chem. C* **2009**, *113*, 19369–19372.

[9] Hong, S. Y.; Tobias, G.; Al-Jamal, K. T.; Ballesteros, B.; Ali-Boucetta, H.; Lozano-Perez, S.; Nellist, P. D.; Sim, R. B.; Finucane, C.; Mather, S. J.; Green, M. L. H.; Kostarelos, K.; Gavis, G. B. Filled and glycosylated carbon nanotubes for *in vivo* radioemitter localization and imaging. *Nat. Mater.* **2010**, *9*, 485–490.

[10] Belluci, S.; Chiaretti, M.; Onorato, P.; Rossella, F.; Grandi, M. S.; Galinetto, P.; Sacco, I.; Micciulla, F. Micro-Raman study of the role of sterilization on carbon nanotubes for biomedical applications. *Nanomedicine* **2010**, *5*, 209–215.

[11] Skakalova, V.; Hulman, M.; Fedorko, P.; Lukáĉ, P.; Roth, S. Effect of gamma-irradiation on single-wall carbon nanotube paper. *AIP Conf. Proc.* **2003**, *685*, 143–147.

[12] Skakalova, V.; Dettlaff-Weglikowska, U.; Roth, S. Gamma-irradiated and functionalized single wall nanotubes. *Diamond Relat. Mater.* **2004**, *13*, 296–298.

[13] Aitkaliyeva, A.; McCarthy, M. C.; Martin, M.; Fu, E. G.; Wijesundera, D.; Wang, X.; Chu, W.; Jeong, H.; Shao, L. Defect formation and annealing kinetics in ion irradiated carbon nanotube buckypapers. *Nucl. Instrum. Meth. Phys. Res. B* **2009**, *267*, 3443–3446.

[14] Cress, C. D.; Schauerman, C. M.; Landi, B. J.; Messenger, S. R.; Raffaelle, R. P.; Walters, R. J. Radiation effects in single-walled carbon nanotube papers. *J. Appl. Phys.* **2010**, *107*, 014316.

[15] Tang, X. W.; Yang, Y.; Kim, W.; Wang, Q.; Qi, P.; Dai, H.; Xing, L. Measurement of ionizing radiation using carbon nanotube field effect transistor. *Phys. Med. Biol.* **2005**, *50*, N23.

[16] Vitusevich, S. A.; Sydoruk, V. A.; Petrychuk, M. V.; Danilchenko, B. A.; Klein, N.; Offenhäusser, A.; Ural, A.; Bosman, G. Transport properties of single-walled carbon nanotube transistors after gamma radiation treatment. *J. Appl. Phys.* **2010**, *107*, 063701.

[17] Memisoglu-Bilensoy, E.; Hincal, A. A. Sterile, injectable cyclodextrin nanoparticles: Effects of gamma irradiation and autoclaving. *Intl. J. Pharm.* **2006**, *311*, 203–208.

[18] Maksimenko, O. O.; Pavlov, E. P.; Tushov, É. G.; Molin, A. A.; Stukalov, Y. U.; Prudskova, T. N.; Sveshnikov, P. G.; Kreuter, J.; Gel'perina, S. É. Radiation sterilization of medicinal formulations of doxorubicin bound to poly(butylcyanoacrylate) nanoparticles. *Pharm. Chem. J.* **2008**, *42*, 363–367.

[19] Smith, B. W.; Luzzi, D. E. Electron irradiation effects in single wall carbon nanotubes. *J. Appl. Phys.* **2001**, *90*, 3509–3515.

[20] Krasheninnikov, A. V.; Banhart, F.; Li, J. X.; Foster, A. S.; Nieminen, R. M. Stability of carbon nanotubes under electron irradiation: Role of tube diameter and chirality. *Phys. Rev. B* **2005**, *72*, 125428.

[21] Zheng, M.; Jagota, A.; Strano, M. S.; Santos, A. P.; Barone, P.; Chou, S. G.; Diner, B. A.; Dresselhaus, M. S.; McLean, R. S.; Onoa, G. B.; Sansibudzem, G. G.; Semke, E. D.; Usrey, M.; Walls, D. J. Structure-based carbon nanotube sorting by sequence dependent DNA assembly. *Science* **2003**, *302*, 1545–1548.

[22] Fagan, J. A.; Simpson, J. R.; Bauer, B. J.; Lacerda, S. H. D.; Becker, M. L.; Chun, J.; Migler, K. B.; Hight Walker, A. R.; Hobbie, E. K. Length-dependent optical effects in single-wall carbon nanotubes. *J. Am. Chem. Soc.* **2007**, *129*, 10607–10612.

[23] Liu, J.; Hersam, M. C. Recent developments in carbon nanotube sorting and selective growth. *MRS Bull.* **2010**, *35*, 315–321.

[24] Green, A. A.; Duch, M. C.; Hersam, M. C. Isolation of single-walled carbon nanotube enantiomers by density differentiation. *Nano Res.* **2009**, *2*, 69–77.

[25] Franç, A.; Pelaz, B.; Moros, M.; Sánchez-Espinel, C.; Hernández, A.; Fernández-López, C.; Grazú, V.; de la Fuente, J. M.; Pastoriza-Santos, I.; Liz-Marzán, L. M.; González-Fernández, A. Sterilization matters: Consequences of different sterilization techniques on gold nanoparticles. *Small* **2010**, *6*, 89–95.

[26] Bozdag, S.; Dillen, K.; Vandervoort, J.; Ludwig, A. The effect of freeze-drying with different cryoprotectants and Gamma-irradiation sterilization on the characteristics of cipro-floxacin HCl-Ioaded poly(D,L-Iactide-glycolide) nanoparticles. *J. Pharm. Pharmacol.* **2005**, *57*, 699–707.

[27] Vauthier, C.; Bouchemal, K. Methods for the preparation and manufacture of polymeric nanoparticles. *Pharm. Res.* **2009**, *26*, 1025–1058.

[28] Schmelling, D. C.; Poster, D. L.; Chaychian, M.; Neta, P.; Silverman, J.; Al-Sheikhly, M. Degradation of polychlorinated biphenyls induced by ionizing radiation in aqueous micellar solutions. *Environ. Sci. Technol.* **1998**, *32*, 270–275.

[29] Becker, M. L.; Fagan, J. A.; Gallant, N. D.; Bauer, B. J.; Bajpai, V.; Hobbie, E. K.; Lacerda, S. H.; Migler, K. B.; Jakupciak, J. P. Length-dependent uptake of DNA-wrapped single-walled carbon nanotubes. *Adv. Mater.* **2007**, *19*, 939–945.

[30] Sayes, C. M.; Fortner, J. D.; Guo, W.; Lyon, D.; Boyd, A. D.; Ausman, K. D.; Tao, Y. J.; Sitharaman, B.; Wilson, L. J.; Hughes, J. B.; West, J. L.; Colvin, V. L. The differential cytotoxicity of water-soluble fullerenes. *Nano Lett.* **2004**, *4*, 1881–1887.

[31] Bachilo, S. M.; Strano, M. S.; Kittrell, C.; Hauge, R. H.; Smalley, R. E.; Weisman, R. B. Structure-assigned optical spectra of single-walled carbon nanotubes. *Science* **2002**, *298*, 2361–2366.

[32] Zeisler, R.; Paul, R. L.; Oflaz Spatz, R.; Yu, L. L.; Mann, J. L.; Kelly, W. R.; Lang, B. E.; Leigh, S. D.; Fagan, J. Elemental analysis of a single-wall carbon nanotube candidate reference material. *Anal. Bioanal. Chem.* **2010**, DOI: 10.1007/s00216-010-4275-6.

[33] Wenseleers, W.; Vlasov, I. I.; Goovaerts, E.; Obraztsova, E.; Lobach, A. S.; Bouwen, A. Efficient isolation and solubilization of pristine single-walled nanotubes in bile salt micelles. *Adv. Funct. Mater.* **2004**, *14*, 1105–1112.

[34] Haggenmueller, R.; Rahatekar, S. S.; Fagan, J. A.; Chun, J.; Becker, M. L.; Naik, R. R.; Krauss, T.; Carlson, L.; Kadla, J. F.; Trulove, P. C.; Fox, D. F.; DeLong, H. C.; Fan, Z.; Kelley, S. O.; Gilman, J. W. Comparison of the quality of aqueous dispersions of single wall carbon nanotubes using surfactants and biomolecules. *Langmuir* **2008**, *24*, 5070–5078.

[35] Welsher, K.; Liu, Z.; Sherlock, S. P.; Robinson, J. T.; Chen, Z.; Daranciang, D.; Dai, H. A route to brightly fluorescent carbon nanotubes for near-infrared imaging in mice. *Nat. Nanotechnol.* **2009**, *4*, 773–780.

[36] Simpson, J. R.; Fagan, J. A.; Becker, M. L.; Hobbie, E. K.; Hight Walker, A. R. The effect of dispersant on defects in length-separated single-wall carbon nanotubes measured by Raman spectroscopy. *Carbon* **2009**, *47*, 3238–3241.

[37] Tsyboulski, D. A.; Bakota, E. L.; Witus, L. S.; Rocha, J. D. R.; Hartgerink, J. D.; Weisman, R. B. Self-assembling peptide coatings designed for highly luminescent suspension of single-walled carbon nanotubes. *J. Am. Chem. Soc.* **2008**, *130*, 17134–17140.

[38] McDonald, T. J.; Engtrakul, C.; Jones, M.; Rumbles, G.; Heben, M. J. Kinetics of PL quenching during single-walled carbon nanotube rebundling and diameter-dependent surfactant interactions. *J. Phys. Chem. B* **2006**, *110*, 25339–25346.

[39] Zhao, J.; Park, H.; Han, J.; Lu, J. P. Electronic properties of carbon nanotubes with covalent sidewall functionalization. *J. Phys. Chem. B* **2004**, *108*, 4227–4230.

[40] Lee, J.; Song, W.; Jang, S. S.; Fortner, J. D.; Alvarez, P. J. J.; Cooper, W. J.; Kim, J. Stability of water-stable C_{60} clusters to OH radical oxidation and hydrated electron reduction. *Environ. Sci. Technol.* **2010**, *44*, 3786–3792.

[41] Boess, C.; Bögl, K. W. Influence of radiation treatment on pharmaceuticals—a review; akaloids, morphine derivatives, and antibiotics. *Drug Dev. Pharm.* **1996**, *22*, 495–529.

[42] Siitonen, A. J.; Tsyboulski, D. A.; Bachilo, S. M.; Weisman, R. B. Surfactant-dependent exciton mobility in single-walled carbon nanotubes studied by single-molecule reactions. *Nano Lett.* **2010**, *10*, 1595–1599.

[43] Dresselhaus, M. S.; Dresselhaus, G.; Avouris, P. *Carbon Nanotubes: Synthesis, Structure, Properties, and Applications*; Springer-Verlag: Heidelberg, 2001.

[44] Suzuki, S.; Kobayashi, Y. Diameter dependence of low-energy electron and photon irradiation damage in single-walled carbon nanotubes. *Chem. Phys. Lett.* **2006**, *430*, 370–374.

[45] Spinks, J. W. T.; Woods, R. J. *An introduction to Radiation Chemistry;* Ch. 7; Wiley Interscience: New York, NY, 1990.

[46] Certain equipment, instruments or materials are identified in this paper in order to adequately specify the experimental details. Such identification does not imply recommendation by the National Institute of Standards and Technology nor does it imply the materials are necessarily the best available for the purpose.

[47] Fagan, J. A.; Becker, M. L.; Chun, J.; Hobbie, E. K. Length fractionation of carbon nanotubes using centrifugation. *Adv. Mater.* **2008**, *20*, 1609–1613.

[48] Fagan, J. A.; Becker, M. L.; Chun, J.; Nie, P.; Bauer, B. J.; Simpson, J. R.; Walker, A. R. H.; Hobbie, E. K. Centrifugal length separation of carbon nanotubes. *Langmuir* **2008**, *24*, 13880–13889.

[49] Zeisler, R.; Lindstrom, R. M.; Greenberg, R. R. Instrumental neutron activation analysis: A valuable link in chemical metrology. *J. Radioanal. Nucl. Chem.* **2005**, *263*, 315–319.

[50] Sambrook, J.; Russel, D. W. *Molecular Cloning: A Laboratory Manual.* 3rd edition; Cold Spring Harbor Laboratory Press: Woodbury NY, 2001.

[51] Fantini, C.; Jorio, A.; Santos, A. P.; Peressinotto, V. S. T.; Pimenta, M. A. Characterization of DNA-wrapped carbon nanotubes by resonance Raman and optical absorption spectroscopies. *Chem. Phys. Lett.* **2007**, *439*, 138–142.